Molecular Crystals and Liquid Crystals
Publication details, including instructions for authors and subscription information:
http://www.tandfonline.com/loi/gmcl16

Density of States in TTF-TCNQ Measured by Inelastic Neutron Scattering

R. Almairac [a], J. L. Prefaut [a], M. Galtier [b], C. Benoit [a], A. Montaner [b] & H. J. Lauter [c]

[a] Laboratoire de Physique, Moléculaire et cristalline, MONTPELLIER Cedex, France

[b] Laboratoire d'Infrarouge, Groupe de dynamique des Phases condensées⊕, (LA 233), USTL 34060, MONTPELLIER Cedex, France

[c] Institut Max Von Laue-Paul Langevin, 156 X centre de tri, 38042, GRENOBLE Cedex, France

Version of record first published: 20 Apr 2011.

To cite this article: R. Almairac , J. L. Prefaut , M. Galtier , C. Benoit , A. Montaner & H. J. Lauter (1981): Density of States in TTF-TCNQ Measured by Inelastic Neutron Scattering, Molecular Crystals and Liquid Crystals, 69:3-4, 177-191

To link to this article: http://dx.doi.org/10.1080/00268948108072699

Mol. Cryst. Liq. Cryst., 1981, Vol. 69, pp. 177–191
0026-8941/81/6903-0177/$06.50/0

Printed in the United States of America

Density of States in TTF—TCNQ Measured by Inelastic Neutron Scattering

R. ALMAIRAC,† J. L. PREFAUT,† M. GALTIER,‡
C. BENOIT,† A. MONTANER‡

†*Laboratoire de Physique Moléculaire et cristalline.*
‡*Laboratoire d'Infrarouge, Groupe de dynamique des Phases condensées*[⊕] *(LA 233), USTL 34060 MONTPELLIER Cedex, France.*

and

H. J. LAUTER

Institut Max Von Laue-Paul Langevin, 156 X centre de tri, 38042 GRENOBLE Cedex France

(*Received June 17, 1980; in final form November 7, 1980*)

The scattering law $\zeta(\omega)$ of TTF—TCNQ at 77K has been measured between 35 and 455 meV (280–3670 cm^{-1}) by inelastic neutron scattering. The data have been corrected for background then deconvoluted by a resolution function established for the spectrometer IN1-B (I.L.L.) and for a powder sample. They are finally compared to the infrared and Raman measurements available.

INTRODUCTION

This work is concerned with the experimental determination of the dynamical properties of TTF—TCNQ by inelastic neutron scattering. The starting point of this study is a better understanding of the high frequency conductivity mechanisms in TTF—TCNQ. In a model for the conductivity based on small polarons hopping,[1] it was predicted that one would expect a strong correlation between the optical conductivity and the one phonon density of states in TTF—TCNQ. In order to check this prediction we have measured the inelastic neutron cross section of TTF—TCNQ in the frequency range 280–3670 cm^{-1}.

Physics Abstracts: 61-10D, 72-15N
[⊕]associated to CNRS

In a first section we describe in details the methods used to correct for background and to deconvolute the data. To this purpose we establish a resolution function for the spectrometer IN1-B (Institut Laue-Langevin-Grenoble). We present a summary of deconvolution in the case of TTF—TCNQ at 77K. The second section is a brief discussion of the results obtained. The infrared and Raman measurements[2-5] of vibrational modes in TTF—TCNQ are recalled for comparison. A more detailed discussion about TTF—TCNQ dynamics will be soon presented in another paper.

I MEASUREMENTS AND DATA PROCESSING

The sample, consisting in 3.16 g of non deuterated TTF—TCNQ crystalline powder, was put in the form of an homogeneous coat sealed in an aluminium envelope. Its thickness was calculated so as to get a total scattering cross section of 10%. The differential cross section, which is essentially incoherent, was measured on the spectrometer IN1-B (hot source of the reactor) by scanning

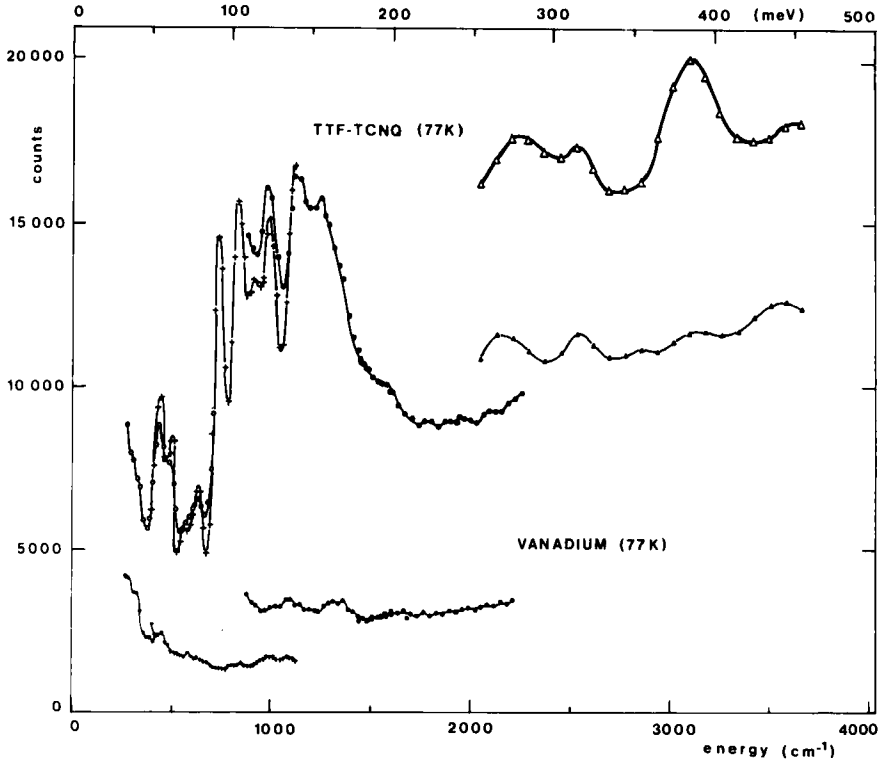

FIGURE 1 *Measured spectrum of TTF—TCNQ at 77K.* The energy ranges of the different monochromators overlap. The lower curve represents the vanadium spectrum.

the incoming energy. In order to cover the whole range from 35 to 455 meV, we have used successively the (111), (002) (220) and (331) Braag reflexions of the copper monochromator by rotating the crystal around a vertical axis parallel to the [1$\bar{1}$0] direction. The scattering angle at the sample was maintained at a constant value of 40 degrees. The beryllium filter in front of the detector was cooled to liquid nitrogen temperature in order to increase its efficiency.

In order to determine the background the sample was replaced by a sheet of Vanadium with the same total cross section of 10%. The Figure 1 shows the TTF—TCNQ and Vanadium spectra.

Background subtraction

The discordance of measurements in the energy overlap ranges, for instance 250–280 meV, is due to the change in geometry when a monochromator is substituted to another. Unfortunately a simple subtraction of the vanadium curve from that of TTF—TCNQ is insufficient to give a satisfactory correction. Consequently we had to find an analytical statement for background giving a more coherent corrected spectrum. Figure 2, which shows the background per

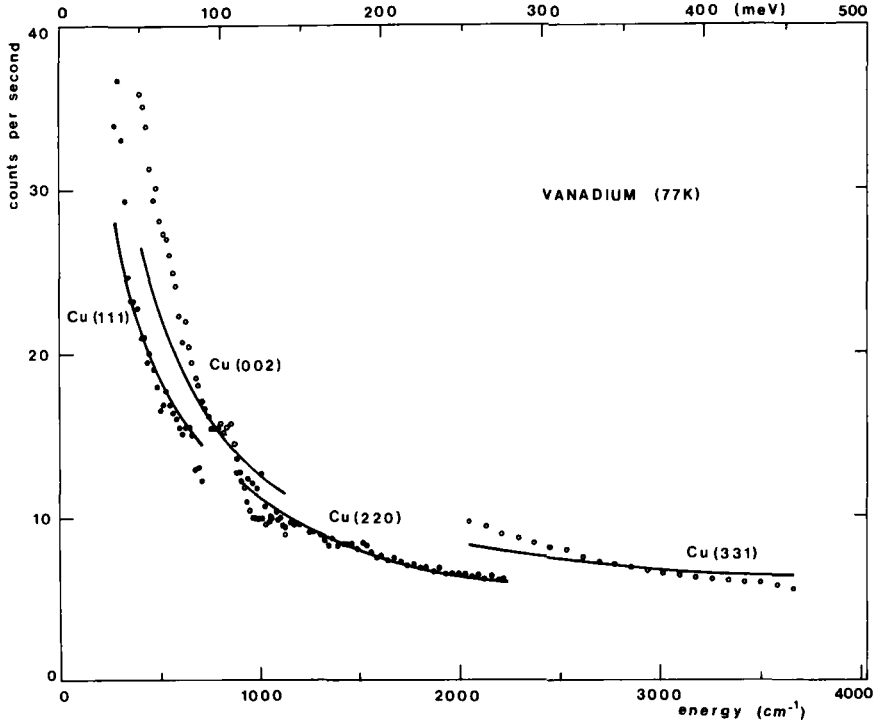

FIGURE 2 *Background per second (vanadium).* The curves are calculated by the expression (1) in which $b = 0$ and $\alpha = 0.80$.

second for the four reflexions of the monochromator, gives the key of this expression. We assume the background per second to be of the form:

$$B = \frac{A_i}{\omega^\alpha} + b. \tag{1}$$

Where

B represents the background per second,
ω represents initial energy,
b represents the surrounding background per second,
A_i is connected to the geometry of the monochromator and depends only on the Braag reflexion used,
α is a real.

The best agreement with the measured data is obtained with $b = 0$ and $\alpha = 0.80$. The A_i parameters were calculated in such a way as to realize a continuity all over the corrected TTF—TCNQ spectrum. The full determination of the four A_i parameters is based upon four conditions: the three conditions on corrected spectra overlaps to which we have associated an additional condition by assuming that at 440 meV, the corrected spectrum is zero. We thus obtain the spectrum in Figure 3.

RESOLUTION FUNCTION

The calculation of the resolution function of the apparatus is derived from the method previously used by Dorner[6] for the three axis spectrometers. According to this author, the number of neutrons reaching the detector per second is:

$$J = \int_{V_I}\int_{V_F} A(k_i)\zeta\left\{\mathbf{k}_i - \mathbf{k}_f, \frac{\hbar}{2m_N}(k_i^2 - k_f^2)\right\}p(\mathbf{k}_i)dv_i p(\mathbf{k}_f)dv_f \tag{2}$$

Where: $\mathbf{k}_i$ and $\mathbf{k}_f$ are the neutron wave vectors before and after the sample (see Figure A-1 in appendix 1) $A(k_i) = A(T)e^{-k_i^2/2k_T^2}$ reflects the dependance of the source spectrum with the heavy water temperature. $p(\mathbf{k}_i)$ is the probability for a neutron coming from the source with a wave vector $\mathbf{k}_i$ to reach the sample. $p(\mathbf{k}_i)$ is given by Dorner's formula (33); $dv_i = dk_{ix}dk_{iy}dk_{iz}$, $p(\mathbf{k}_f)$ is the probability for a neutron coming from the sample with a wave vector $\mathbf{k}_f$ to pass through the Beryllium filter and to be detected. $dv_f = dk_{fx}dk_{fy}dk_{fz}$,

$$\zeta\left\{\mathbf{k}_i - \mathbf{k}_f, \frac{\hbar}{2m_N}(k_i^2 - k_f^2)\right\}$$

is the scattering law $\zeta(\mathbf{Q},\omega)$ where $\mathbf{Q} = \mathbf{k}_i - \mathbf{k}_f$, $\omega = (\hbar/2m_N)(k_i^2 - k_f^2)$, $\zeta(\mathbf{Q},\omega)$ is related to the inelastic neutron cross section by:

$$\zeta(\mathbf{Q},\omega) = \frac{k_i}{k_f}\frac{d^2\sigma}{d\Omega d\omega}$$

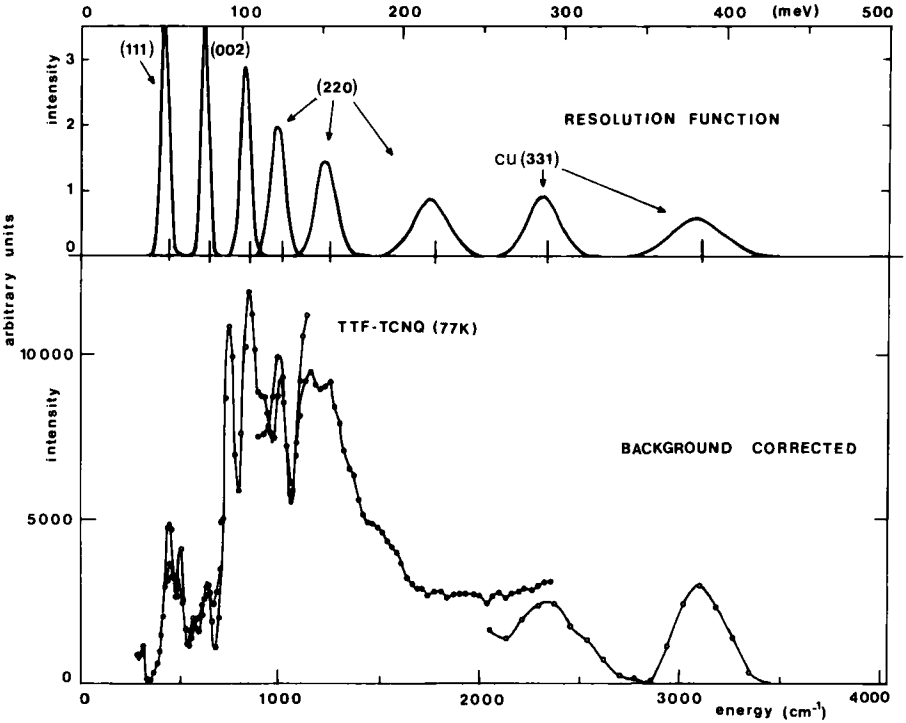

FIGURE 3 *TTF—TCNQ spectrum at 77K corrected for background.* The upper part of the figure shows the change of the resolution function (calculated) along the whole energy range.

The function $p(\mathbf{k}_f)$ also brings in the energy response of the beryllium filter for which we chose a gaussian:

$$e^{-\frac{(\hbar^2/2m_N)^2 k_f^4}{2\alpha_{Be}^2}},$$

Where α_{Be} characterizes the filter's energy cut-off. The reason for this somewhat arbitrary choice was its simplicity. Note that this function can represent the *Be* filter response only if the integration on k_f is restricted to the positive range. The detailed calculation of the function $p(\mathbf{k}_f)$ is given in appendix 1.

The number of neutrons reaching the monitor per second is given by:

$$J_0 = \int_{V_I} k_i A(k_i) p(\mathbf{k}_i) dv_i \tag{3}$$

A measurement performed with a monitor preselection, when the spectrometer is set on the incoming energy E_I:

$$E_I = \frac{\hbar^2}{2m_N} k_I^2 = \hbar\omega_0,$$

gives the ratio:

$$I(\omega_0) = k_I \frac{J(\omega_0)}{J_0} \tag{4}$$

Where

$$\mathbf{Q}_0 = \mathbf{k}_I - \mathbf{k}_F,$$

with $\mathbf{k}_I$ = initial mean wave vector,
and $\mathbf{k}_F$ = final mean wave vector selected by the beryllium filter.

The energy dependance of the monitor efficiency has been taken into account through the term in k_I in (4).

Changing to the sample variables, $\mathbf{Q}$ and ω, one gets

$$J(\omega_0) = \int_\omega \int_Q \zeta(\mathbf{Q},\omega) F(\mathbf{Q} - \mathbf{Q}_0,\ \omega - \omega_0)\, d\mathbf{Q}\, d\omega \tag{5-A}$$

with

$$F(\mathbf{Q} - \mathbf{Q}_0, \omega - \omega_0) = \int_{V_I} \int_{V_F} A(k_i) p(\mathbf{k}_i) p(\mathbf{k}_f)\, \delta[\mathbf{Q} - (\mathbf{k}_i - \mathbf{k}_f)]$$

$$\times\, \delta\left[\omega - \frac{\hbar}{2m_N}(k_i^2 - k_f^2)\right] dv_i\, dv_f \tag{5-B}$$

Since sample is a crystal powder, $\zeta(\mathbf{Q},\omega)$ shown in (5-A) actually represents an average over all the possible orientations of the axes of a TTF—TCNQ cell and depends only on $|\mathbf{Q}|$. On the other hand, since $\mathbf{Q}$ takes its values in a volume $\Delta\mathbf{Q}$ (Figure A-1), which is large compared to the volume of the reciprocal cell of TTF—TCNQ, the wave vector of the scattering process measured ($\mathbf{q} + 2\pi\tau = \mathbf{Q}$ for a one phonon scattering), takes all possible values in the Brillouin zone (for example at 150 meV $\Delta Q \sim 0.85\ \text{Å}^{-1}$ whereas $a^* = 1.65\ \text{Å}^{-1}$, $b^* = 0.51\ \text{Å}^{-1}$ and $c^* = 0.34\ \text{Å}^{-1}$; the condition $\Delta Q \geqslant a^*/2, b^*/2, c^*/2$ is realized). As a result, the measurement can only give an average function $\zeta(\mathbf{Q},\omega)$ which we call $\tilde{\zeta}(\mathbf{Q}_0,\omega)$. The expression of $J(\omega_0)$ then becomes:

$$J(\omega_0) = \int_\omega \tilde{\zeta}(Q_0,\ \omega)\tilde{F}(Q_0,\ \omega - \omega_0) d\omega \tag{6}$$

Where we have introduced:

$$\tilde{F}(Q_0, \omega - \omega_0) = \int_Q F(\mathbf{Q} - \mathbf{Q}_0, \omega - \omega_0) d\mathbf{Q} \tag{7}$$

We define the resolution function $R(Q_0, \omega - \omega_0)$ using (4) and (6):

$$I(\omega_0) = \int_\omega \tilde{\zeta}(Q_0, \omega) R(Q_0, \omega - \omega_0)\, d\omega \tag{8-A}$$

with

$$R(Q_0, \omega - \omega_0) = \frac{k_I}{J_0} \tilde{F}(Q_0, \omega - \omega_0) \tag{8-B}$$

We obtain (notations specified in appendix 1):

$$R(Q_0, \omega - \omega_0)$$

$$= \mathfrak{N} \frac{tg\theta_M}{k_I^2 \nu} \int_0^\infty e^{-1/2\{tg^2\theta_M/\nu^2[(\omega/\omega_0 + \hbar k_I^2/2m_N\omega_0)^{1/2} - 1]^2 + k_I^4/0.232\alpha_{Be}^2\}} k_f^2 dk_f \tag{9}$$

Where θ_M and k_I depends on ω_0.

The calculation of $R(Q_0, \omega - \omega_0)$ includes a numerical integration coming from the beryllium filter response. The angular widths of the beams which come in $R(Q_0, \omega - \omega_0)$ through the geometrical factor ν have been expressed as function of $k_I (k_I \propto \omega_0^{1/2})$ due to the displacement of the monochromator. The only parameters to introduce in the calculation of the resolution are thus the effective widths of the source, monochromator and sample, the mosaic spread η_M of the monochromator and the energy width of the Beryllium filter. The isolated peaks in the measured spectrum allow us to adjust these parameters taking into account the fact that the apparatus function cannot be larger than the measured peaks.

Several examples of the resolution function calculated by this method are given in Figure 3, while Figure 4 shows the calculated width for the four monochromators on the whole spectrum. Note the small energy shift of the resolution function from the value $\omega_0 (\sim 3$ meV) originated from the Beryllium filter response (Figure 3). The instrumental width goes from 5 to 40 meV when ω_0 runs from 40 to 420 meV, despite the fact that in relative value, the resolution keeps a fairly constant value of 9% (from 7% to 11%). The Cu (200) has a much better resolution than monochromators Cu (111) et Cu (220), this being confirmed by the data (77 meV and 123 meV peaks in Figure 3). The same applies to Cu (331) which has a better resolution than Cu (220) in the energy overlap range.

DECONVOLUTION

To proceed on to deconvolution, we adjusted a theoretical curve $\tilde{\zeta}(Q_0, \omega)$ to the background corrected spectrum $J(\omega_0)$ by a method of least squares. $\tilde{\zeta}(Q_0, \omega)$ is not an analytical function, however in order to perform the adjustment we have approximated $\tilde{\zeta}(\omega)$ by an analytical function $\tilde{\zeta}_{\text{analy}}(Q_0, \omega, \delta\omega)$ near every frequency: this approximation is expected to be valid in a frequency range

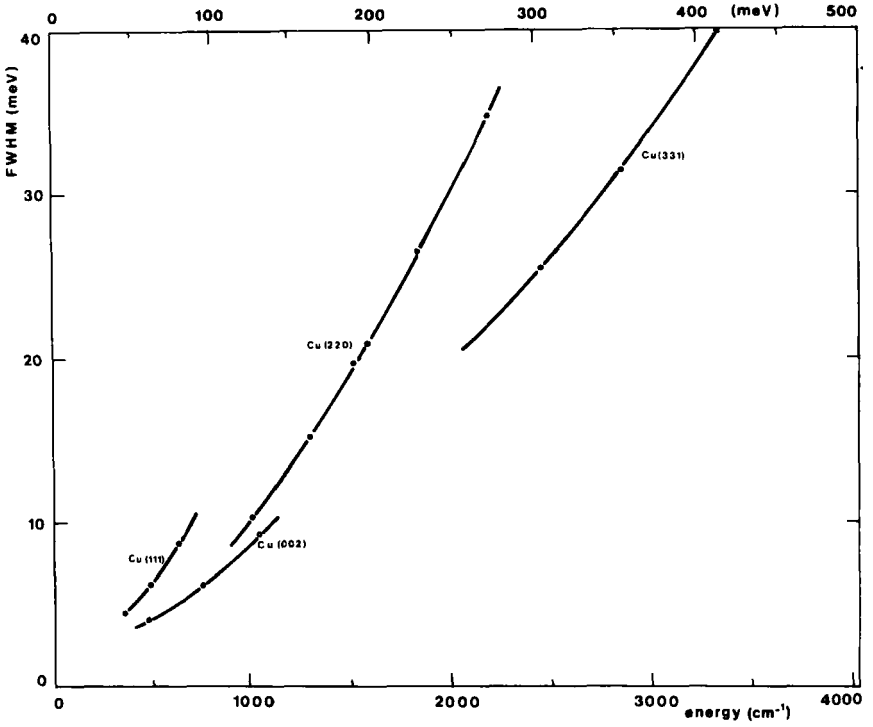

FIGURE 4 *Variation of the width* of the resolution function (FWHM), along the whole energy range.

equal to twice the resolution width around ω. The set of functions $\tilde{\zeta}_{\text{analy}}(Q_0, \omega, \delta\omega)$ obtained by this method allows us to construct the function

$$\tilde{\zeta}(Q_0, \omega) = \tilde{\zeta}_{\text{analy}}(Q_0, \omega, 0)$$

which constitutes the deconvoluted spectrum. We choose for $\tilde{\zeta}(Q_0, \omega, \delta\omega)$ the sum of two "Lorentzians" whose widths were fixed at 1.5% of ω, the amplitude and position being the free parameters of the fit. Thus, we get the curve on Figure 5. The choice of Lorentzians (rather than any other function) can seem arbitrary so we checked that the set of points $\tilde{\zeta}(Q_0, \omega)$ directly convolved to the resolution function gives back the background corrected spectrum.

Geneally speaking, stronger is the peak, smaller are the error bars on the position and on the force (area). Our analysis does not permit to yield in a precise way the width of the lines. However we note on this curve, that the adjustment method used does not restrict the value of the linewidths. An example is given by the peaks at 90 meV and 102 meV which, although very close, have very different widths (2.5 meV and 3.7 meV).

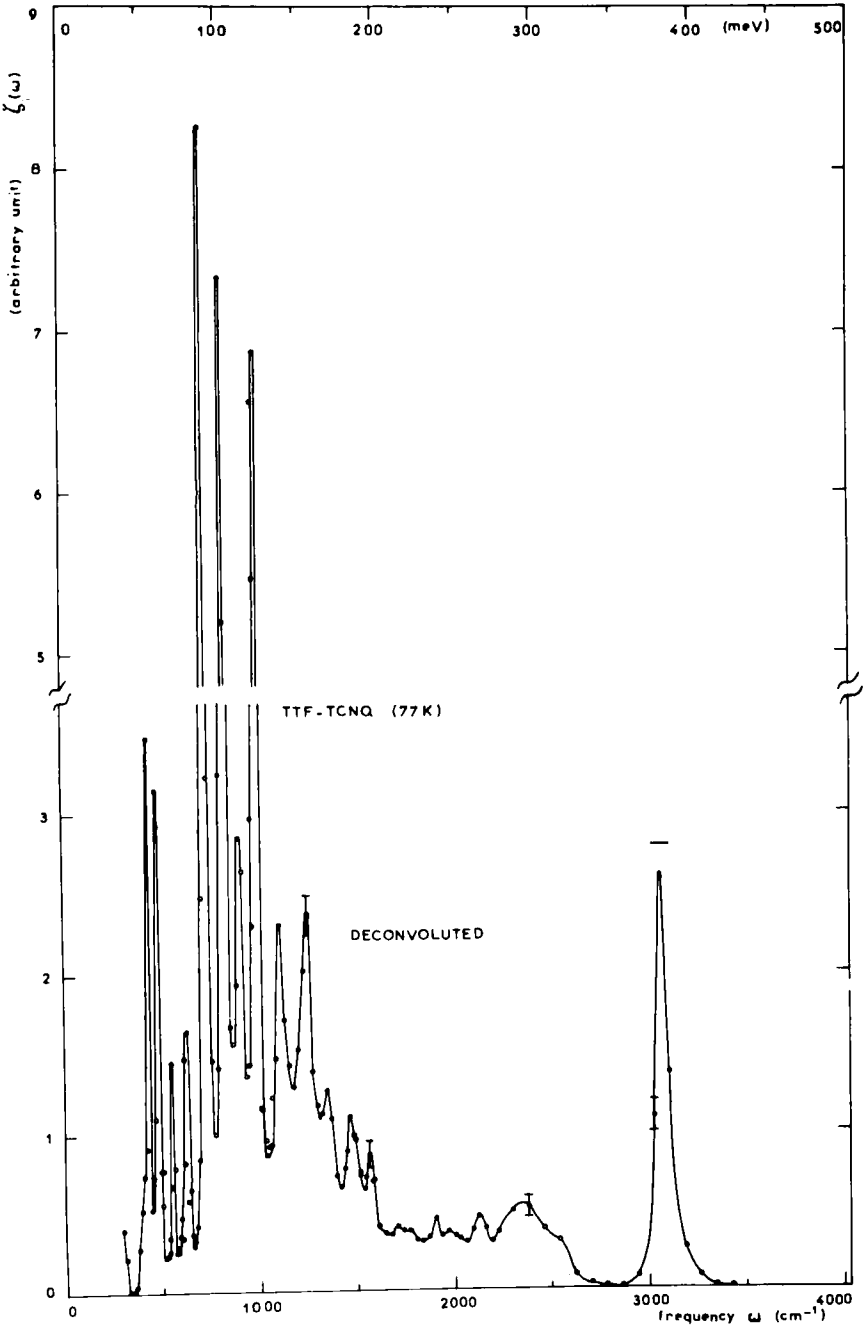

FIGURE 5 *Deconvoluted spectrum of TTF—TCNQ at 77K.* Some error bars are indicated: the vertical segment stands for the estimated amplitude error, while the horizontal segment stands for the estimated error on frequency.

II DISCUSSION

The scattering law on Figure 5, which we will henceforth call $\zeta(\omega)$ has a very complex structure. We can nevertheless distinguish three regions. In the region from 320 to 1620 cm^{-1}, $\zeta(\omega)$ shows a basis whose intense and very broad

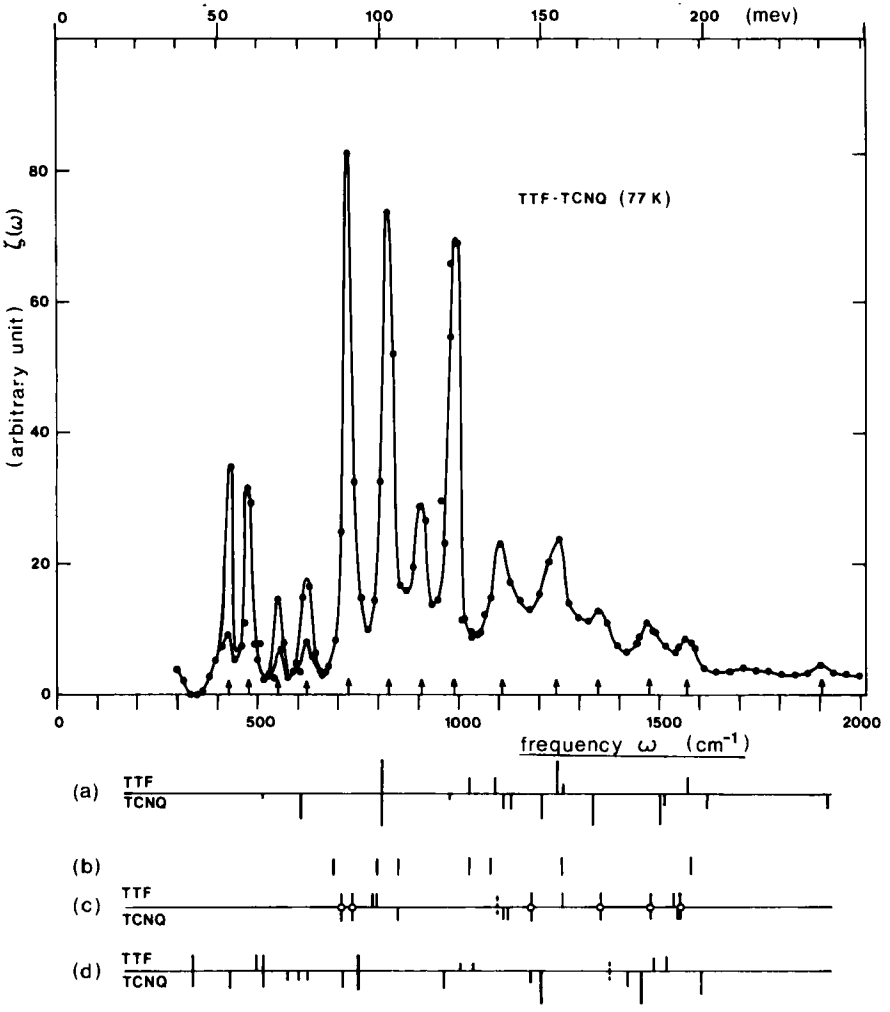

FIGURE 6 *Scattering law $\zeta(\omega)$ of TTF—TCNQ at 77K compared with the infrared and Raman results.* The infrared results are indicated on (a), (b) and (c), taken from references (2), (3) and (4), respectively. The Raman bands (d) are taken from the paper of Kuzmany *et al.* (5). Assignments: bands assigned to TTF are above the horizontal line, bands assigned to TCNQ are below; dashed lines = not assigned; bands marked with a circle are assigned to the complex. The length of the lines indicates the strength: v.w., w., m., s., v.s. . . . The arrows below the $\zeta(\omega)$ curve indicate the positions of the peaks measured at half maximum.

maximum is centered around 1130 cm^{-1}, on this basis are superimposed well defined lines, the strongest of which is situated at 725 cm^{-1}. The 1620 to 2820 cm^{-1} intermediate region presents a basis with no precise structure and whose amplitude is much weaker than the former. We distinguish only a very broad peak centered at about 2280 cm^{-1} (the shoulder at 2500 cm^{-1} on the side of this peak is probably due to a defect in background correction). The very intense peak centered at 3080 cm^{-1} constitutes the third region.

For the interpretation of $\zeta(\omega)$ we will limit the discussion to a brief comparison with the infrared and Raman results (Figure 6). Infrared absorption spectra at room temperature were measured by different authors with different experimental conditions,[2-4] giving bands whose frequencies fairly rarely coincide. The bands determinated by Aharon-Shalom *et al.* in infrared on monocrystal as well as the Raman scattering lines measured on monocrystal by Kuzmany *et al.*[5] are indicated with their strengths and their assignments. Let us not that, since these optical spectra are sensible only to the zone center modes it is somewhat illusory to look for a peak to peak coincidence of $\zeta(\omega)$ with infrared and Raman measurements. Furthermore, since hydrogen has a very strong incoherent scattering cross section, we practically see through $\zeta(\omega)$ only the vibration modes inferring displacements of the hydrogens. We can thus explain the very strong amplitude of the peak corresponding to the C—H stretching mode at 3080 cm^{-1} in excellent agreement with the determination of Aharon-Shalom *et al.* We can also understand why the second region, which is the region of the CN group vibrations, does not include any intense peak. Finally, let us note that the first region of $\zeta(\omega)$ corresponds fairly well to the group of the lines determined by Aharon-Shalom and Kuzmany.

In detail, no precise correlation between the peaks of $\zeta(\omega)$ and those obtained by optical methods can be established. It is evident that, up to this point an assignment of the maxima of $\zeta(\omega)$ is necessary. A more complete discussion using measurements performed with TTF alone, TCNQ alone, as well as the present measurements will be presented in another paper.

Acknowledgments

We express our gratitude to L. Giral and J. M. Fabre for the synthesis as well as to J. L. Ribet for the purification of the products. We have pleasure to thank B. Dorner for useful comments on the resolution function.

References

1. C. Benoit, M. Galtier, and A. Montaner, *Phys. Stat. Sol.*, (b) **91**, 269 (1979).
2. E. Aharon-Shalom, M. Weger, I. Agranat and E. Wiener-Avnear, *Sol. State. Comm.*, **23**, 53 (1977).
3. C. Benoit, M. Galtier, A. Montaner, J. Deumie, H. Robert and J. M. Fabre, *Solid State Comm.*, **20**, 257 (1976).

4. W. T. Wozniak, G. De Pasquali, M. V. Klein, R. L. Sweany and T. L. Brown, *Chem. Phys. Lett.* **33**, 33 (1975).
5. H. Kuzmany and H. J. Stalz, *J. Phys.*, C **10**, 2241 (1977). H. Kuzmany, B. Kundu and H. J. Stalz, Proc. Int. Conf. Lattice Dynamics. Flammarion, Paris 1978, Ed. M. Balkanski.
6. B. Dorner, *Acta Cryst.*, A **28**, 319 (1972).
7. M. J. Cooper and R. Nathans, *Acta Cryst.*, **23**, 357 (1967).

APPENDIX 1

We present a practical formulation of the resolution function defined by:

$$R(Q_0, \omega - \omega_0) = k_I \frac{\tilde{F}(Q_0, \omega - \omega_0)}{J_0} \tag{A-1}$$

where

$$\tilde{F}(Q_0, \omega - \omega_0) = \int_{V_I} \int_{V_F} A(k_i) p(\mathbf{k}_i) p(\mathbf{k}_f) \delta\left[\omega - \frac{\hbar}{2m_N}(k_i^2 - k_f^2)\right] dv_I dv_f \tag{A-2}$$

and

$$J_0 = \int_{V_I} k_i A(k_i) p(\mathbf{k}_i) dv_i \tag{A-3}$$

We characterize each basic element of the spectrometer by its mosaic spreads (η, η') or by their horizontal and vertical angular widths (α, β). From one element to the other the neutron beam is characterized by horizontal γ and vertical δ angular coordinates, by its incident and scattered wave numbers $\mathbf{k}$ and their modulus. The Table I precises these notations for all the elements of the apparatus.

TABLE I

Definition of the angular variables used in the appendix.

	Mosaic spreads	Output angular variables
Source		$\mathbf{k}_1(k_1, \gamma_1, \delta_1)$
Collimator 1	(α_1, β_1)	$\mathbf{k}_2(k_2, \gamma_2, \delta_2)$
Monochromator	(η_M, η'_M)	$\mathbf{k}_3(k_3, \gamma_3, \delta_3)$
Collimator 2	(α_2, β_2)	$\mathbf{k}_i(k_i, \gamma_4, \delta_4)$
Sample	powder	$\mathbf{k}_f(k_f, \gamma_5, \delta_5)$
Be-Filter plus detector	(η_F, η'_F)	

The scattering diagram is schematized on Figure A-1. Taking into account that $k_i = k_I + \Delta k_i \approx k_I$ we obtain with Dorner [(6)-formula (33)]:

$$p(\mathbf{k}_i)dv_I = \frac{\beta_1}{\sqrt{\beta_1^2 + 4\eta'^2_M \sin^2\theta_M}} P_M(k_I^*)\, e^{-1/2[(\gamma_4+2(\Delta k_i/k_I)tg\theta_M/\alpha_1)^2+(\gamma_4+(\Delta k_i/k_I)tg\theta_M/\eta_M)^2 + (\gamma_4/\alpha_2)^2+(1/(\beta_1^2+4\eta'^2_M\sin^2\theta_M)+1/\beta_2^2)S_4^2]} k_I^2 d(\Delta k_i) d\gamma_4 d\delta_4, \quad \text{(A-4)}$$

On the other hand:

$$p(\mathbf{k}_F)dv_F = e^{-\gamma_5^2/2\eta_F^2} e^{-\delta_5^2/2\eta'^2_F} \varphi(k_f) k_f^2\, dk_f d\gamma_5 d\delta_5. \quad \text{(A-5)}$$

We consider the set Be-filter-detector as a collimator for which the probability of neutron's transit is given by Cooper and Nathans.[7] Furthermore, this probability is limited by the energy acceptance of the beryllium: a good approximation of this function seemed to be a gaussian of the form (at 77K):

$$\varphi(k_f) = e^{-E_f^2/2\alpha_{Be}^2} = e^{-k_f^2/0.465\alpha_{Be}^2} (E_f \text{ in meV and } k_f \text{ in } \text{Å}^{-1}), \quad \text{(A-6)}$$

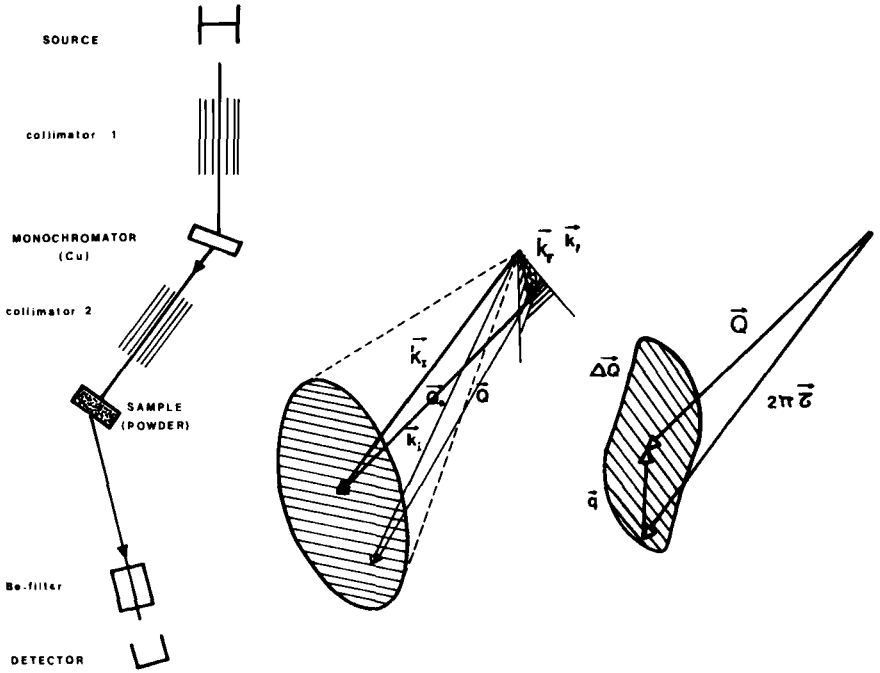

FIGURE A-1 Experimental setting of IN1-B and drawing of the scattering process in the reciprocal space.

where α_{Be} corresponds to $\varphi(E_f) = 1/2$ for $E_f = 2.5$ meV.

Calculation of I_0: After integration of A-3 over δ_4, γ_4, and $\Delta k_i/k_I$, and if we set:

$$\frac{1}{\lambda^2} = \frac{1}{\alpha_1^2} + \frac{1}{\eta_M^2} + \frac{1}{\alpha_2^2}, \frac{1}{\mu^2} = \frac{2}{\alpha_1^2} + \frac{1}{\eta_M^2},$$

and

$$\frac{1}{\nu^2} = \frac{4}{\alpha_1^2} + \frac{1}{\eta_M^2} - \frac{\lambda^2}{\mu^4},$$

we have:

$$J_0 = A(T)P_M(k_I)k_I^4 e^{-k_i^2/2k_I^2} \frac{(2\pi)^{3/2}\beta_1\beta_2}{\sqrt{\beta_1^2 + \beta_2^2 + 4\eta_M'^2 \sin^2\theta_M}} \frac{\lambda\nu}{tg\theta_M}. \quad \text{(A-7)}$$

Calculation of $F(Q_0, \omega_0, \omega - \omega_0)$: After integration of A-2 over δ_5, γ_5, δ_4 and γ_4, and eliminating the variable k_i, through Dirac's distribution, taking into account that $k_i^2 = 2m_N\omega/\hbar + k_f^2$ and $k_I^2 = 2m_N\omega_0/\hbar$, one is left with:

$$\Omega = \int_{k_f=0}^{\infty} e^{-1/2\{tg^2\theta_M/\nu^2[(\omega+(\hbar k_f^2/2m_N)/\omega_0)^{1/2}-1]^2 + k_f^2/0.232\alpha_{Be}^2\}} k_f^2 dk_f, \quad \text{(A-8)}$$

then,

$$\tilde{F}(Q_0, \omega - \omega_0)$$

$$= \hbar N A(T)P_M(k_I)k_I e^{-k_i^2/2k_I^2} \frac{(2\pi)^2\eta_F\eta_F'\lambda\beta_1\beta_2}{\sqrt{\beta_1^2 + \beta_2^2 + 4\eta_M'^2 \sin^2\theta_M}} \cdot \Omega, \quad \text{(A-9)}$$

where N is the number of cells in the sample.

We finally obtain, according to A-1, the following expression of $R(Q_0, \omega - \omega_0)$:

$$R(Q_0, \omega - \omega_0) = \mathfrak{N} \frac{tg\theta_M}{k_I^2\nu} \cdot \Omega \quad \text{(A-10)}$$

where $\mathfrak{N}$ is a normalization factor, k_I and θ_M are functions of ω_0:

$$\theta_M = \text{Arc sin } 1.252 \sqrt{\frac{h^2 + k^2 + l^2}{\omega_0}} \text{ (for the Cu)} \quad \text{(A-11)}$$

The analytical calculation of Ω, possible under some assumptions, leads to a complicated expression of $R(Q_0, \omega - \omega_0)$. So, it is more advisable to retain the form (A-8) which can be easily calculated by a numerical integration.

The fact that we have used four different reflexions of the copper monochromator from one hand of the spectrum to the other, and that, furthermore, the geometry of the diffractometer varies with the energy for a given reflexion

of the monochromator, leads to the following expressions of the widths α_1 and α_2:

$$\alpha_1 = \text{Arc } tg\left[\frac{l_s + l_m \cos(\beta_m - \theta_M)}{L_{sd} - L/tg(2\theta_M)}\right] \tag{A-12}$$

$$\alpha_2 = \text{Arc } tg\left[\sin(2\theta_M)\frac{(l_e + l_m \cos(\beta_m + \theta_M))}{L}\right] \tag{A-13}$$

where

L = meter

l_s is the radius of the source

l_m the half-width of the monochromator

β_m expresses the calculated variation of the efficient area of the monochromator as a function of the Braag reflexion used.

Face	(111)	(002)	(220)	(331)
β_m (rad)	0.616	1.571	0.000	0.231

l_e is the half-width of the sample,

L_{sd} is the distance source-detector projected on the axis source-monochromator.